Mixtures of soft and rigid grains: an experimental approach

Manuel Cárdenas-Barrantes, Jonathan Barés, Mathieu Renouf, Emilien Azéma

Mixtures of soft and rigid grains: an experimental approach

M. Cárdenas-Barrantes [a], J. Barés [a], M. Renouf [a], and E. Azéma [a,b]

a. LMGC, Université de Montpellier, CNRS, Montpellier, France - manuel-antonio.cardenas-barrantes@umontpellier.fr
b. Institut Universitaire de France (IUF), Paris, France

Résumé :

Dans bien des cas, les milieux granulaires sont composés de grains avec des propriétés mécaniques très différentes. Nous étudions expérimentalement la compaction de systèmes bidisperses 2D constitués de particules molles et rigides, et analysons également l'évolution de leurs principaux observables macroscopiques tout au long de la compaction. L'analyse est faite depuis l'état lâche jusqu'à des densités très élevées, bien au-delà du blocage, en suivant les modifications à l'échelle locale pour chaque particule du système. Nous exposons les principales caractéristiques du comportement de ces systèmes dans chacune des différentes phases (lâche, bloquée et dense) et leur variations à la traversée des zones de transition. Cette étude constitue la première étape vers une meilleure compréhension du comportement mécanique des matériaux granulaires polydisperses en termes de rhéologie des grains.

Abstract :

Granular systems can be composed of grains of very different mechanical properties. Experimentally, we study the compaction of 2D bidisperse systems made of soft and rigid particles and analyze the evolution of their main macroscopic observables during the compaction. The analysis is made from the quasi-loose state, passing through the jamming transition up to very high densities. Regarding the local (particle scale) and the global scale (macroscopic system), we show the main characteristics in the behavior of such a system, when each phase (rigid or soft) is dominant and what is the main character in the transition. This study constitutes the first step toward a better understanding of the mechanical behavior of granular materials that are polydisperse in terms of grain rheology.

Keywords: Granular matter, Soft granular compaction, High deformation

1 Introduction

Homogeneous assemblies of soft granular media are involved in a wide variety of natural and industrial processes, such as biological tissues composed of soft cells [11], suspensions [15], clayey materials [5, 13], and any sintered material [8, 10]. However, it has been shown that the mixture of materials with different elastic properties, such as soft and rigid particles, gives rise to new and fascinating mechanical effects. These outcomes include better stress relaxation [9], foundation damping [6, 9], and seismic

isolation [14, 16]. All without compromising the macroscopic mechanical stability of the material. The amount of stiff or soft particles that are added to these composite materials is generally chosen in an empiric manner, therefore, a more precise study of these composites for their optimization is necessary.

The effect of adding soft particles to rigid ones must be understood from the particles and contact scale, looking at how each particle deforms and what their contribution is to the whole system as a bulk. Experimentally, the measurement of local mechanical properties is a great challenge and even more in this case where the particles exceed the limit of the small deformation regime, which most measurement methods take as a basis [1]. In this study, we use a recently developed experimental method that employs Digital Image Correlation methods coupled with very accurate imaging. This permits to measure these large deformations at the particle scale relying on the resolution of the imaging [17].

The communication is structured as follows. In Section 2, we briefly describe the experimental approach followed during the compaction and also the image analysis procedure. In Section 3, we present the main results of this study. Here we differentiate the macro-mechanical and micro-mechanical aspects of the compaction. Finally, conclusions are presented in Section 4.

2 Experimental set up and image processing

The experiment consists of a bidimensional piston of initial dimension (270×202) mm^2 which compresses oedometrically a bidisperse assembly of rigid and soft cylinders randomly placed on top of a flatbed scanner. The loading piston is composed of a stepper motor rotating a screw that moves the edge of the piston in the inward direction and two force sensors (Figure 1.(a)). The force is measured with a frequency of 100 Hz, and the pressure P is directly computed ($P = \sigma_{yy}$ by convention). The compressed cylinders are made of hyperelastic silicone and rigid PVC with Young's moduli $E = 0.7$ MPa and 1.2 GPa, respectively. PVC and Silicone cylinders both have a size bidispersity with diameters of 20 mm and 30 mm and a height of 15 mm. In both cases the Poisson ratio is close to 0.5. For each loading step, the piston moves by 0.5 mm steps with a speed of 2 mm/min to assure being in the quasistatic regime. Then, the system is imaged from below with a resolution of 2400 dpi (10.6 μm/px). For each experiment, about $N = 100$ particles are used keeping the ratio between rigid and soft particles $\kappa = \mathrm{N_{soft}}/\mathrm{N}$ constant. This ratio is equally spread among soft and rigid particles and varies in the set $\kappa \in [0.2, 0.5, 0.8, 1.0]$. To avoid basal friction, the scanner glass is coated with oil which also lubricates the contacts between particles, making them virtually frictionless. The bottom of each particle is painted with thin metallic glitter, which creates a random pattern with a correlation length of approximately 50 μm [17]. Figure 1.(c) shows the evolution of the measured force as a function of the global strain ε for different mixture ratios.

For each experiment, a set of about 90 pictures shows the evolution of the compaction. These pictures are post-processed with a DIC algorithm modified from [4, 17, 18]. First, each particle center is detected on the initial undeformed image and then tracked from one image to the next one getting their solid-rigid motion. Second, for the soft particles, the displacement field for each particle i at each step n is obtained $(\mathbf{u}(\mathbf{x}, \mathbf{y})_{\mathbf{i}}^{\mathbf{n}})$. The deformation gradient tensor is then computed: $\mathbf{F} = \nabla \mathbf{u} + \mathbf{I}$, with $\mathbf{I}$ the second-order identity tensor. Then, From $\mathbf{F}$ the right Cauchy-Green strain tensor field, $\mathbf{C} = \mathbf{F^T F}$, and the von Mises strain, $\mathcal{C}$, are deduced. For the rigid particles, the local stresses are too low to induce any significant deformation of the PVC, so we assume that they do not deform. Finally, contacts between particles are measured from the proximity of the boundaries and the von Mises strain. Fig. 1.(b) shows the von Mises strain field toghether with the scan of a granular sample with $\kappa = 0.5$.

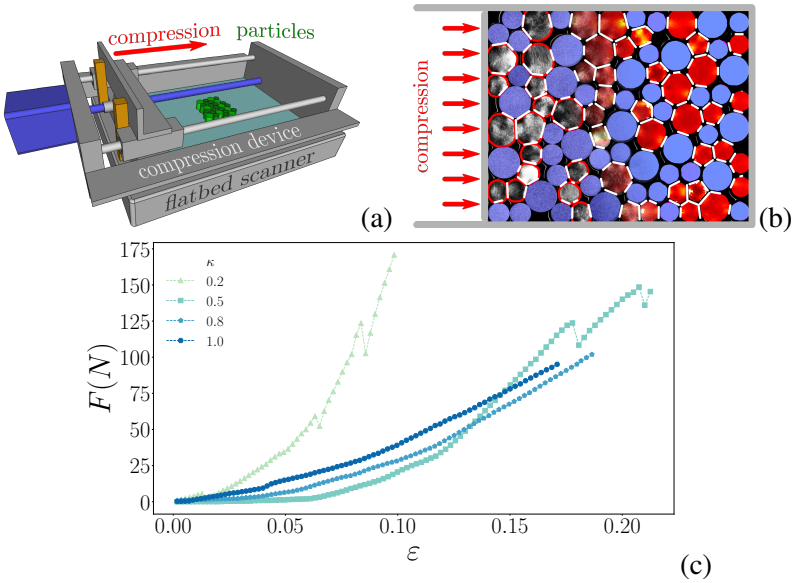

Figure 1: (a) Experimental set-up. (b). Composite view of measured fields. All rigid particles are colored in blue. Raw image, in gray level, is shown on the left, particle boundaries are in red. Von Mises strain field is shown on the right with a color scale going from dark red (low value) to yellow (high value). Contacts are shown in white. (c) Evolution of the measured force, F, as a function of the global strain, ε, for different values of mixture κ.

3 Results and discussions

3.1 Macromechanical aspects

Figure 2 shows the evolution of the main macroscopic quantities of the system. On one side, we show the packing fraction, ϕ, defined as the ratio between the particles and the particles' container volume, as a function of the applied pressure directly calculated from the measured force. On the other side, the coordination number, Z, quantifying the average number of neighbors per particle, is shown as a function of the packing fraction. The previous quantities are presented relatively to the packing fraction ϕ_0 and coordination number Z_0 at the jammed state. We have selected the jamming transition point where the system can support a non-negligible load, $P_c = 1$ kPa in our case. At this fixed point P_c, ϕ_0 takes the values $(0.83, 0.83, 0.81, 0.78)$, and Z_0 takes the values $(3.31, 3.50, 3.25, 3.30)$ for the mixture ratios $(0.2, 0.5, 0.8, 1.0)$, respectively.

In Fig.2(a), the packing fraction evolves with the same general trend regardless of κ. It first increases with P from ϕ_0 and then tends asymptotically to a maximum packing fraction ϕ_{max}, which clearly depends on κ. Together with the evolution of the compaction, Fig. 2(a) also shows a previously developed micro-mechanical model, based on the evolution of the stress tensor and without *ad-hoc* parameters, to describe the evolution [3]. This model gets excellent predictions for the different values of κ, except for $\kappa = 0.2$ for which minor discrepancies are observed, even if the general tendency is reproduced. In this latter case, we can invoke finite size-effect and sharp particle rearrangements due to the small number of soft grains.

In Fig.2(b), as has been systematically reported in the literature, Z increases following a power-law, $Z - Z_0 = \xi(\phi - \phi_0)^\alpha$, with $\alpha \sim 0.5$ and ξ a structural parameter fully defined as $P \to \infty$. Both ϕ and Z reach a maximum value ϕ_{max} and Z_{max}, respectively. This relation was observed both numerically

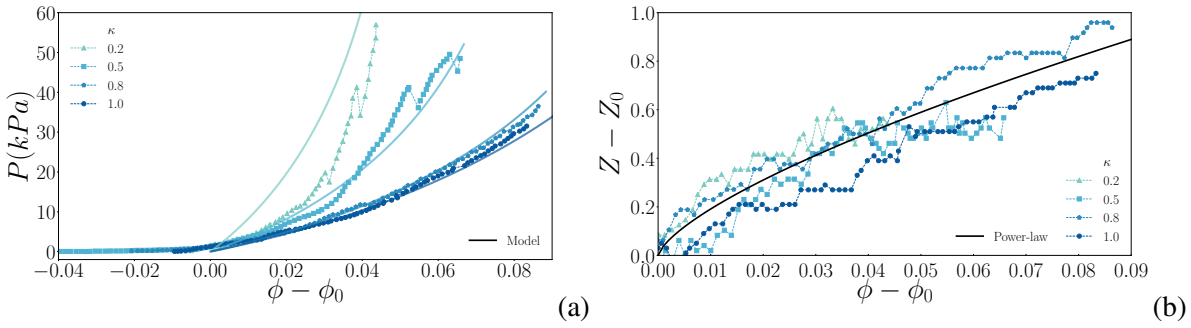

Figure 2: (a) Evolution of the global stress applied to the system, P, as a functions of $\phi - \phi_0$ for different mixture ratio κ. Plain curves correspond to the micro-mechanical model presented in [3] (b) Evolution of the excess coordination number, $Z - Z_0$, with $Z_0 \approx 3.8$, as a function of the excess packing fraction, $\phi - \phi_0$ for different mixtures ratios κ. The solid line is the power-law relation $Z - Z_0 = \xi(\phi - \phi_0)^\alpha$, with $\alpha = (0.7 \pm 0.15)$ and its uncertainty value taken from the numerical regression.

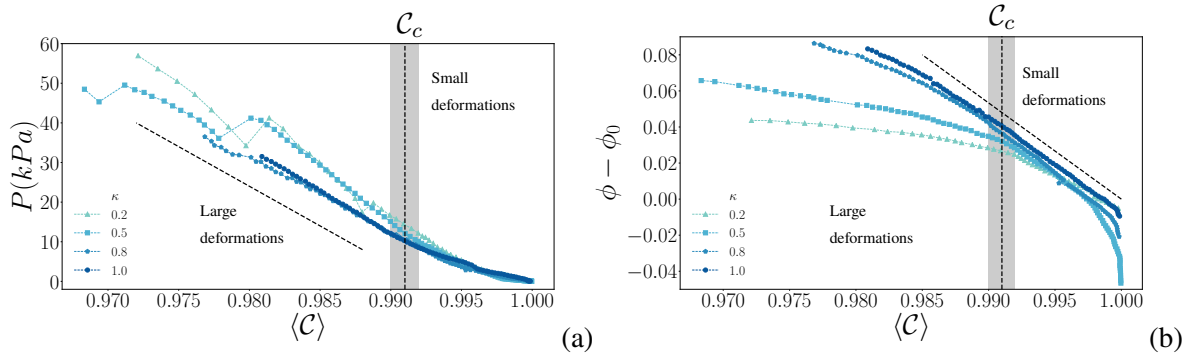

Figure 3: (a),(b): Evolution of the global stress, P, and of the excess of packing fraction $\phi - \phi_0$, as a function of the average value of the von Mises strain, $\langle \mathcal{C} \rangle$ in soft particles, for different κ values. In (a) and (b) the straight black dashed lines display linear regimes. The vertical gray line and the shaded area shows the critical strain $\mathcal{C}_c = 0.991 \pm 1.2 \times 10^{-3}$ and its errorbar, respectively. It splits the space horizontally between large and small particles' deformation regimes.

and experimentally for many granular assemblies like foams, emulsions, and rubber-like particles [2, 7, 17]. All the curves collapse fairly well on the power-law relation. Although the exponent α is slightly overestimated, within the error bars, we are in the same domain of $\alpha \approx 0.5$. This large error bar is mainly due to the smallness of the system.

3.2 Microstructural aspects

It is then possible to relate the strain inside the particles to macroscopic observables. Under the small deformation assumption the infinitesimal strain tensor, ε, is related to the Cauchy-Green strain tensor by $\varepsilon = 1/2(\mathbf{C} - \mathbf{I})$. In a compressed bulk material, this strain tensor and the global stress and strain are linearly related. Since deep in the jammed state, the material has a density close to the bulk, one can wonder if this relation is still observed.

As seen in Fig. 3(a) and (b), when the system is compressed, the mean von Mises strain $\langle \mathcal{C} \rangle$ inside soft particles decreases from 1 while the pressure and the packing fraction increase. At low compaction level, for $\langle \mathcal{C} \rangle > \mathcal{C}_c \approx 0.991$, it decreases linearly with the packing fraction regardless of the mixture ratio, $\langle \mathcal{C} \rangle \sim \phi - \phi_0$. For a higher level of compression, it leaves this linear regime decreasing more

rapidly for higher values of κ. It is worth noting that in the linear regime, all curves collapse in a single one regardless of the mixture ratio. On the contrary, at a high compression level, for $\langle \mathcal{C} \rangle < \mathcal{C}_c$, the mean von Mises strain decreases linearly with the global pressure except for some noise due to the particle rearrangements, $\langle \mathcal{C} \rangle \sim P$. For low deformation levels, all curves collapse on a parabolic curve. In the first regime ($\langle \mathcal{C} \rangle > \mathcal{C}_c$), the linearity is reminiscent of the one observed between the global strain scale and the packing fraction, being still in a rigid regime. In the second regime ($\langle \mathcal{C} \rangle > \mathcal{C}_c$), the linearity between the local strain and the global stress suggests that the material behaves like a bulk. This is consistent with the material's low porosity. It is also consistent with the fact that, at large compression levels, the pressure decreases faster with the strain for lower mixture ratio: the material gets stiffer for lower κ. On the contrary, in small compression levels, linear relations collapse and do not significantly depend on the mixture ratio.

4 Conclusions

We analyzed experimentally the oedometric compaction of granular assemblies composed of mixtures of both rigid and soft cylindrical particles. First, these experimental results validate a previously developed compaction model for the case of the oedometric compaction of a quasi-two-dimensional system. Second, we confirmed the power-law tendency for the excess coordination number as a function of the excess packing fraction. However, the exponent is slightly overestimated from the one reported in the literature, which is mainly due to the small size of the system. Finally, we found that the average strain inside soft particles evolves linearly with the packing fraction, while in the case of high loading levels, it scales with the global pressure applied to the system. This evidences two distinct regimes separated by a critical value independent of κ.

References

[1] A. Abed-Zadeh, J. Barés, T. Brzinski, K. Daniels, J. Dijksman, N. Docquier, H. Everitt, J. Kollmer, O. and Lantsoght, D. Wang, M. Workamp, Y. Zhao, H. Zheng, Enlightening force chains: a review of photoelasticimetry in granular matter, Granular Matter, 21 (2019) 83.

[2] B, Andreotti, Y. Forterre, O. Pouliquen, Granular media: between fluid and solid, Cambridge University press, (2013).

[3] M. Cárdenas-Barrantes, D. Cantor, J. Barés, M. Renouf, E. Azéma, Compaction of mixtures of rigid and highly deformable particles: A micromechanical model, Physical Review E, 3 (2020) 032904.

[4] Python codes to post-process experimental images (particle tracking, DIC, fields computation, https://git-xen.lmgc.univ-montp2.fr/Image/granular_dic

[5] N. Ilieş, V. Farcaş, O. Mureşan, M. Gherman, V. Chiorean, Soil improvement with polyetylene waste materials in order to improve mechanical parameters, International Multidisciplinary Scientific GeoConference: SGEM: Surveying Geology & mining Ecology Management, 17 (2017) 751-758.

[6] B. Indraratna, Y. Qi, T. Ngo, C. Rujikiatkamjorn, T. Neville, F. Bessa-Ferreira, A. Shahkolahi, Use of geogrids and recycled rubber in railroad infrastructure for enhanced performance, Geosciences, 9 (2019) 30

[7] G. Katgert, M. van Hecke, Jamming and geometry of two-dimensional foams, Europhysics Letters, 3 (2010) 34002

[8] K. Kawakita, K. Lüdde, Some considerations on powder compression equations, Powder Technology, 4 (1971) 61-68

[9] H. Khatami, A. Deng, M. Jaksa, The arching effect in rubber-sand mixtures, Geosynthetics International, (2018) 1-58

[10] K. Kim, M. Carroll, Compaction equations for strain hardening porous materials, International Journal of Plasticity, 3 (1987) 63-73

[11] J. Mauer, S. Mendez, L. Lanotte, F. Nicoud, M. Abkarian, G. Gompper, D. Fedosov, low-Induced Transitions of Red Blood Cell Shapes under Shear, Physical Review Letters, 11 (2018) 118103

[12] T. Vu, J. Barés, S. Mora, S. Nezamabadi, Numerical simulations of the compaction of assemblies of rubberlike particles: A quantitative comparison with experiments, Physical Review E, 6 (2019) 062903

[13] M. Rúa, P. Bustamante-Baena, Modeling the mechanical behavior of a kaolin ceramic paste owing to the variation in the particle size, Boletín de la Sociedad Española de Cerámica y Vidrio, 3 (2019) 105-112

[14] K. Senetakis, A. Anastasiadis, K. Pitilakis, Dynamic properties of dry sand/rubber (SRM) and gravel/rubber (GRM) mixtures in a wide range of shearing strain amplitudes, Soil Dynamics and Earthquake Engineering, 33 (2012) 38-53

[15] R. Stannarius, D. Sancho-Martinez, T. Finger, E. Somfai, T. Börzsönyi, Packing and flow profiles of soft grains in 3D silos reconstructed with X-ray computed tomography, Granular Matter, 3 (2019) 56

[16] H. Tsang, Seismic isolation by rubber-soil mixtures for developing countries, Earthquake Engineering & Structural Dynamics, 37 (2008) 283-303

[17] T. Vu, J. Barés, Soft-grain compression : Beyond the jamming point, Physical Review E, 4 (2019) 42907.

[18] T. Vu, J. Barés, S. Mora, S. Nezamabadi, Numerical simulations of the compaction of assemblies of rubberlike particles: A quantitative comparison with experiments, Physical Review E, 6 (2019) 062903.